International Journal of Rock Mechanics & Mining Sciences 126 (2020) 104174

Contents lists available at ScienceDirect

International Journal of Rock Mechanics and Mining Sciences

journal homepage: http://www.elsevier.com/locate/ijrmms

Rockburst prediction and stability analysis of the access tunnel in the main powerhouse of a hydropower station based on microseismic monitoring

Ruixiong Xue [a], Zhengzhao Liang [a,*], Nuwen Xu [b], Linlu Dong [b]

[a] State Key Laboratory of Coastal and Offshore Engineering, Dalian University of Technology, Dalian, 116024, China
[b] State Key Laboratory of Hydraulics and Mountain River Engineering, Sichuan University, Chengdu, Sichuan, 610065, China

ARTICLE INFO

Keywords:
High in situ stress
Microseismic monitoring
Rockburst
Early warning
Shuangjiangkou hydropower station

ABSTRACT

The access tunnel in the main powerhouse of the Shuangjiangkou hydropower station in China has complex geological conditions and is subject to high in situ stress in deep buried sections. Microseismic activity in the surrounding rock mass of the tunnel was monitored by a microseismic monitoring system, and rockburst was effectively predicted. Based on abundant data obtained from the microseismic monitoring, statistical parameters, which include cumulative apparent volume, the energy index, cumulative released energy and the Es/Ep value, were used to analyze the microseismic activity before and after rockburst to determine a more accurate early warning period and construction safety period. A sharp decrease in the energy index and a rapid increase in the cumulative apparent volume indicated a deterioration of the surrounding rock mass stability. The change characteristics of Es/Ep values revealed that the rockburst process underwent a transformation of compression-shear damage, tension-shear mixed damage and tension damage. Finally, based on the number of daily events N and the b value of the microseismic events, lgN/b was first established to evaluate the rockburst risk of tunnels. When the value of lgN/b was greater than 1, rockburst was more likely to occur; the larger the lgN/b value, the more severe the rockburst was. The research results provide an important reference value for the prediction of rockbursts in deep tunnels and the regulation of site construction progress.

1. Introduction

Rockburst is a special failure pattern that occurs during excavation in a high-stress environment, accompanied by the sudden release of strain energy, and it can pose a considerable threat to on-site workers and engineering equipment. Therefore, research on rockburst mechanisms and predictions has become a key scientific and technical pursuit in rock mechanics to reduce and control rockbursts.[1]

Detailed analysis of the occurrence process of rockburst and revealing rockburst mechanisms are the keys to accurately predicting rockbursts. Extensive theoretical and experimental studies have been conducted on failure mechanisms, forecasting methods, and prevention technologies. Ortlepp and Stacey[2] distinguished several different rockburst mechanisms in tunnels and shafts, drew a distinction between source and damage mechanisms, and suggested five rockburst types in tunnels and shafts, namely, strain burst, buckling, face crush burst, shear rupture, and fault slip burst. Their research results form a good foundation for further analysis of rockburst mechanisms and rockburst prediction in underground engineering in the future. Based on research findings from other researchers, Kaiser et al.[3] proposed three rockburst types (strain burst, pillar burst, and fault slip burst). Frid[4] established the electromagnetic radiation criterion for rockburst prediction in coal mines. The antenna that captured signals was normally located 1 m from the mine working face. Therefore, this method of predicting rockbursts cannot be applied to general tunnel excavation. Romashov[5] first proposed a generalized model of rockbursts that was in accordance with the general character of deformations in rock masses and physical representations of many phenomena. Their research results form a good foundation for creating a rockburst model of specific rock masses and developing new more reliable methods of estimating their rockburst hazard. Liu et al.[6] used cloud models and the attribution weight method to predict rockburst classifications. The data collection is an enormous challenge for their applicability. Gong and Li[7] established a distance discriminant analysis method for rockburst prediction. In the research, the parameters used to build the model are difficult to be obtained on site, so it is an enormous challenge for applications in the tunnel with complex geological environments. In fact, rockburst is an extremely complex phenomenon influenced by several factors, including

* Corresponding author.
E-mail address: LiangZZ@dlut.edu.cn (Z. Liang).

https://doi.org/10.1016/j.ijrmms.2019.104174
Received 22 March 2019; Received in revised form 16 October 2019; Accepted 15 December 2019
Available online 28 December 2019

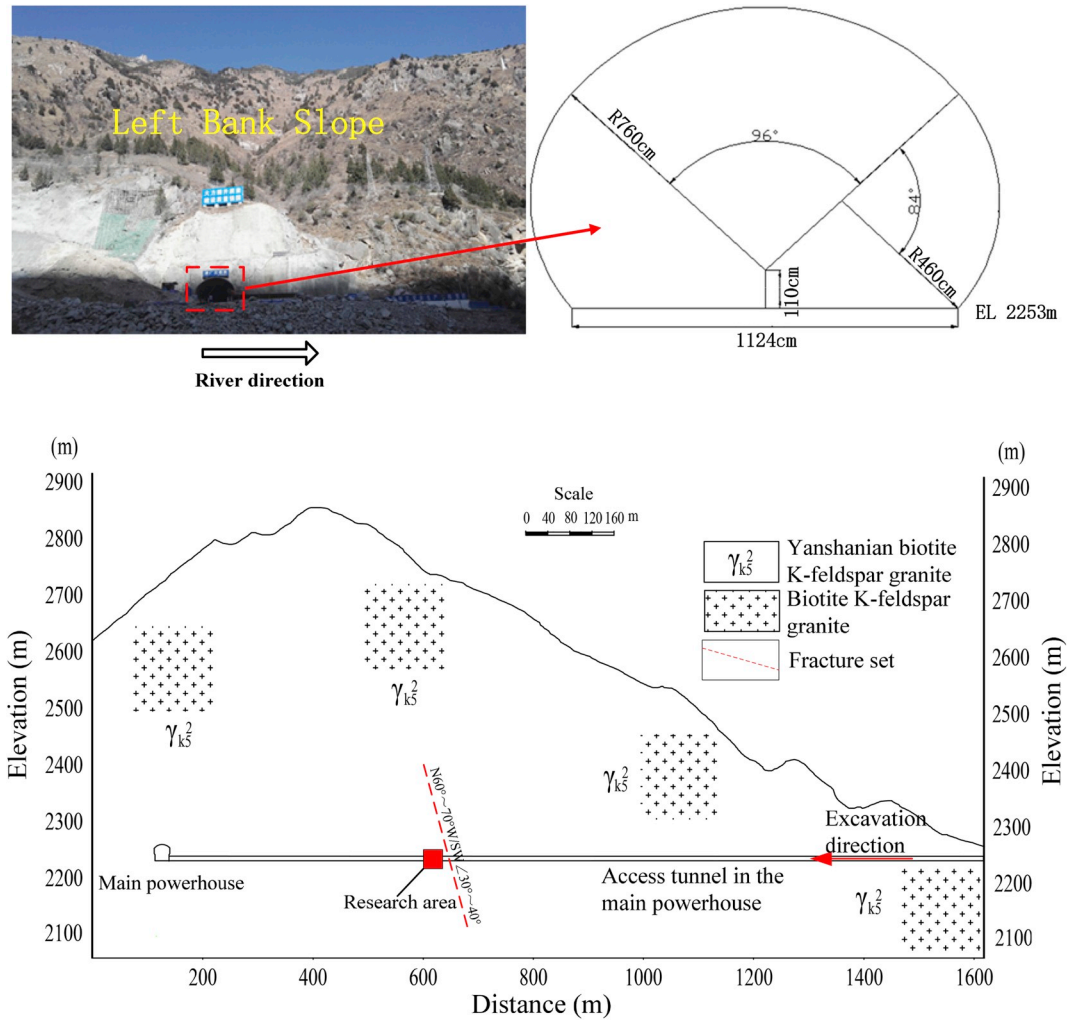

Fig. 1. Left bank slope of Shuangjiangkou hydropower station. a. Photograph of the left bank showing the geological conditions and shape of the access tunnel in the main powerhouse. b. Geological profile of the access tunnel in the main powerhouse.

geological conditions, rock lithology, and tunnel excavation method.

When a rock mass is disturbed by excavation unloading, microfracturing occurs inside the rock mass, accompanied by the release of stored elastic energy in the form of a stress wave, thereby generating microseismic events.[8] In recent years, as a three-dimensional space monitoring technology for monitoring rock mass microfracturing, microseismic monitoring technology has achieved rapid development.[9,10] Using an analysis of stress waves received by microseismic sensors, abundant microseismic source parameters, such as time, space position, energy and moment magnitude, can be obtained; then, the microseismic source parameters, once analyzed and summarized in detail, can reveal the rockburst mechanism and activity law inside the surrounding rock after rockburst. Many researchers have extensively investigated rockburst hazards in recent years with respect to rockburst mechanisms and prediction by microseismic monitoring technology and achieved remarkable results. Feng et al.[11] used real-time microseismic data to provide a dynamic warning method for rockburst risk during excavation of a tunnel. The method in which multiple microseismic parameters were comprehensively analyzed had been successfully applied to rockburst warning in deeply buried tunnels at the Jinping II hydropower project. Therefore, detailed analysis on multiple microseismic parameters is very important to predict rockburst.

Blake et al.[12] found that the MS activity increased abnormally before rockburst induced by roof fracturing in hard-rock mines. Their research results form a good foundation for further analysis of MS activity law based on microseismic monitoring technology. Xiao et al.[13] studied strain-structure slip rockburst evolution mechanisms using moment tensor analysis of microseismic events. A new method, which uses decomposed parts of the moment tensor and the P-wave development factor of the MS events to form a main judgment criterion, can provide a reliable estimate of the rock mass failure type occurring during rockburst evolution. Tang et al.[14] studied the evolution law of the *b* value and concluded that the *b* value exhibits obvious precursor characteristics before rockburst. The *b* value represents the proportional relationship between the number of large magnitude events and the number of small magnitude events. Therefore, the number of events is also very important for rockburst prediction. It is necessary to combine the *b* value and the number of events as an index for rockburst prediction. Xiao et al.[15] studied and evaluated the rockburst risk of a deep tunnel section, where strong rockbursts were experienced, based on microseismic information. It give us a much better understanding of the tunnel excavation behavior and present us with a more satisfactory way of controlling excavation to ensure that engineering is carried out safely.

Yu et al.[16] studied the fractal characteristics of microseismic volume for different types of immediate rockburst in deep tunnels. The immediate rockbursts is that the rockburst occurred in the surrounding rock during the process of excavation unloading effect. The position of the rockburst is close to the working face, and the interval of rockburst time and the excavation time are relatively short. The immediate rockbursts includes immediate strain rockbursts and immediate strain-structure

Table 1
The results of rock mass in-situ stress measurements in geological exploration tunnels.

No.	Measuring points	Measuring point locations	Horizontal depth/m	Vertical depth/m		σ_1	σ_2	σ_3
1	σ_{SPD9-4}	Stake 0 + 115 m in SPD9	115 m	107 m	Value (MPa)	15.98	8.53	3.14
					α(°)	325.6	81.8	208.5
					β(°)	30.1	37.3	38.1
2	σ_{SPD9-3}	Stake 0 + 205 m in SPD9	205 m	173 m	Value (MPa)	22.11	11.63	5.86
					α(°)	332.0	84.0	210.1
					β(°)	30.1	32.9	42.3
3	σ_{SPD9-2}	Stake 0 + 301 m in SPD9	301 m	238 m	Value (MPa)	19.21	13.61	5.57
					α(°)	323.0	49.2	300.4
					β(°)	−23.5	8.6	64.8
4	σ_{SPD9-1}	Stake 0 + 400 m in SPD9	400 m	308 m	Value (MPa)	37.82	16.05	8.21
					α(°)	331.6	54.1	137.7
					β(°)	46.8	−7.0	42.3
5	σ_{SPD9-6}	Stake 0 + 470 m in SPD9	470 m	357 m	Value (MPa)	27.29	18.27	8.49
					α(°)	310.4	36.8	223.8
					β(°)	−3.5	45.6	44.2
6	σ_{SPD9-5}	Stake 0 + 570 m in SPD9	570 m	470 m	Value (MPa)	28.96	18.83	10.88
					α(°)	325.0	72.5	201.4
					β(°)	27.2	30.3	47.0

Note: α is the angle of the principal stress in the horizontal projection. The angle of true north is zero and clockwise rotation. While β is the dip angle of the principal stress, and the angle of elevation is positive.

slip rockbursts. In this study, the authors noted that for immediate strain rockbursts and immediate strain-structure slip rockbursts, if the intensity is lower, the fractal volume dimensions will be smaller; for immediate strain-structure slip rockbursts, the greater the number of structure planes, the smaller the fractal volume dimensions. Since the number of structural planes is uncertain before excavation, it is an enormous challenge for applying the research results to rockburst prediction during the excavation process of tunnel. Chen et al.[17] predicted the occurrence of rockburst in deep tunnels based on the evolution law of the measured energy index and cumulative apparent volume. It shows that it is practicable to predict rockburst by microseismic monitoring technology. Energy index and cumulative apparent volume can be used as indexes for predicting rockbursts.

Various research results have been obtained on rockburst mechanisms and predictions. Due to the complex physical and mechanical properties of rock masses, the triggering effects of geomechanical conditions and the construction factor, the rockburst mechanism is very complicated, and the accurate prediction of rockbursts has always been a difficult problem.[11] At present, the rockburst mechanism is still unclear. As noted by Brown,[18,19] it is difficult to reach an agreement on the definition of rockburst. Therefore, further studies on the microfracturing precursor information of rockbursts and the rockburst mechanism may inspire new ideas in understanding and predicting rockbursts. Moreover, there are few studies on the activity law inside the surrounding rock after the occurrence of a rockburst, even though this is vitally important for the construction safety of the site.

This paper focuses on the rockburst mechanism and the activity law in the surrounding rock mass after a rockburst in an access tunnel in the main powerhouse of the Shuangjiangkou hydropower station, which is located in Sichuan Province, China. The statistical parameters, which include cumulative apparent volume, the energy index, cumulative released energy and the Es/Ep value, were used to analyze microseismic activity before and after the rockburst to determine a more accurate early warning period and construction safety period. The Es/Ep values

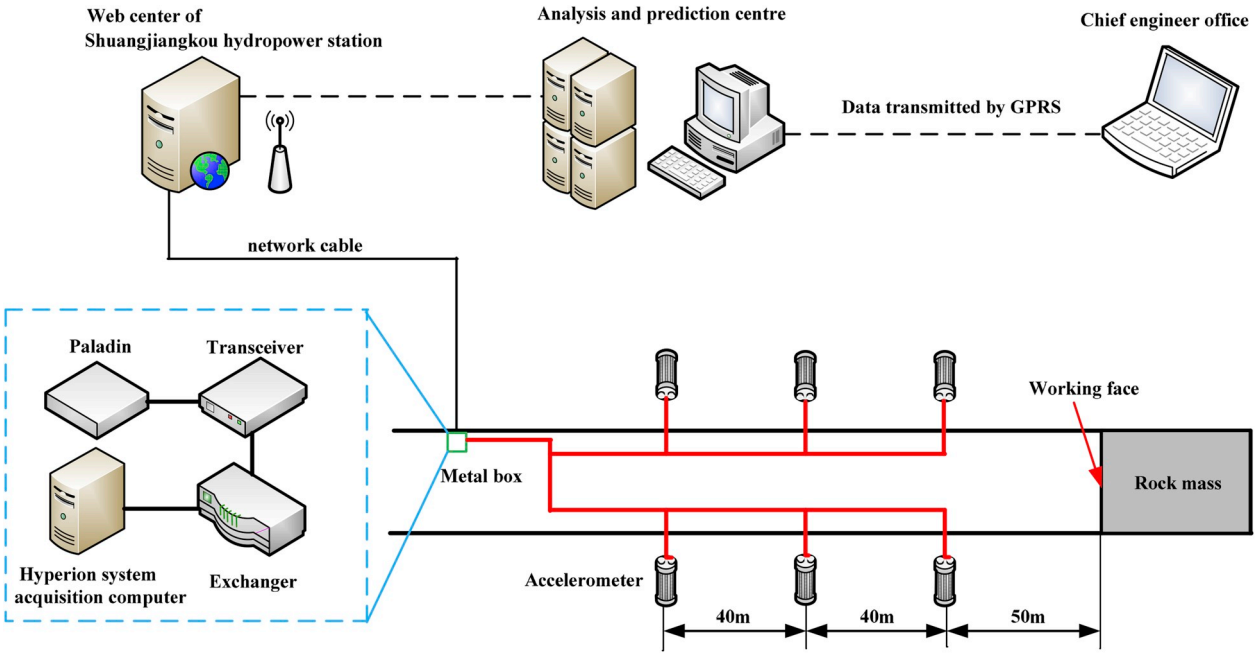

Fig. 2. Microseismic monitoring system topology.

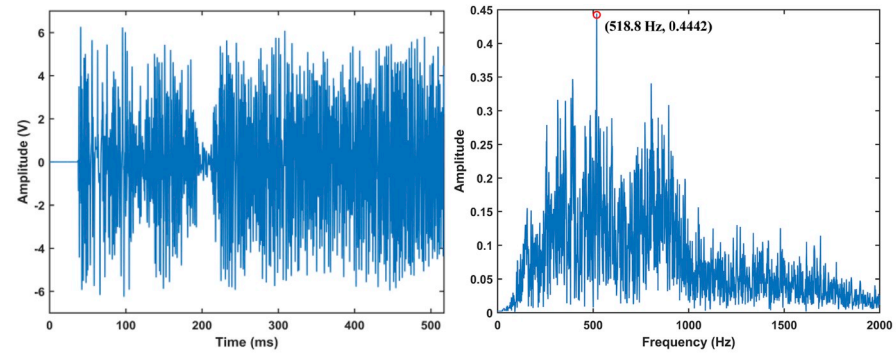

(a) Excavation blasting

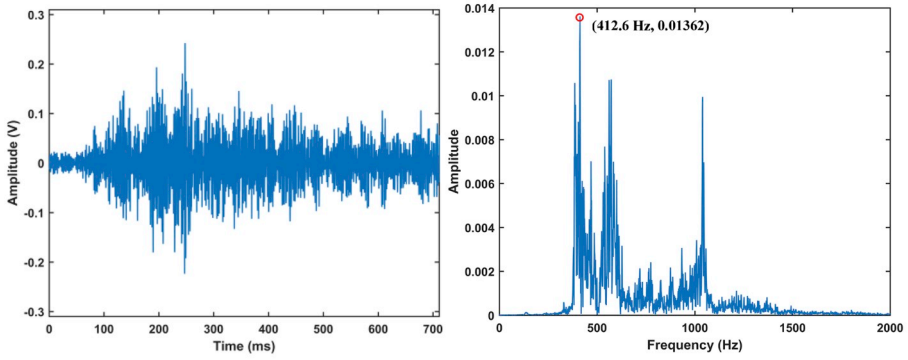

(b) Truck horn

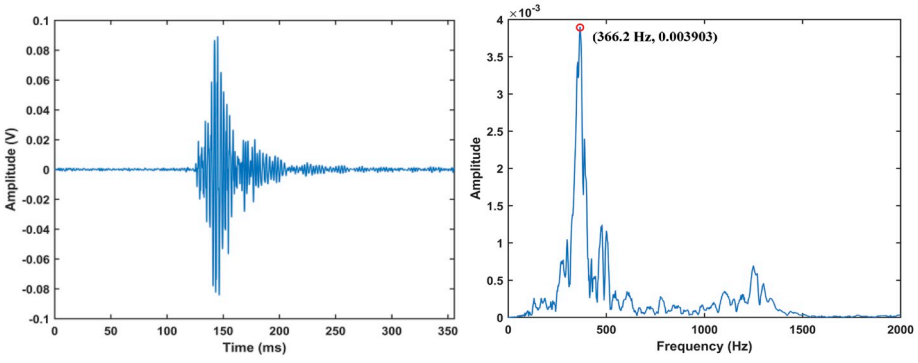

(c) Microseismic event

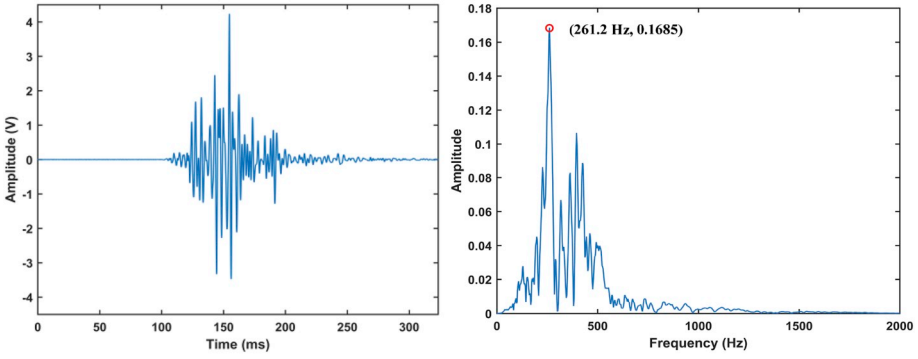

(d) Rockburst

Fig. 3. Waveform analysis of different signals in both the time and frequency domains at the access tunnel in the main powerhouse.

(the ratio of the energy released by the S wave and the P wave) were then implemented to explore the damage types at the different stages. Finally, based on the number of daily events N and the b value of the microseismic events, lgN/b was first established to evaluate the rockburst risk of the surrounding rock mass.

2. Project overview

The Shuangjiangkou hydropower station is a large-scale step hydropower project constructed on the Dadu River. It is located approximately 382 km northwest of Chengdu in Sichuan Province, China. The project was constructed in a V-shaped valley. This project includes a 314-m-tall soil core rockfill dam, which is the world's highest dam of this type and controls a drainage area of more than 39,330 km^2. The reservoir has a normal pool level of 2500 m. The total storage capacity is 2.897 billion m^3 and the adjustment storage capacity is 1.917 billion m^3. The powerhouse can accommodate four 500 MW turbine generators for a total generating capacity of 2000 MW.

The access tunnel in the main powerhouse is arranged on the left bank (Fig. 1). The project region on the left bank, including small-scale faults and joint fissures, is stable overall. The total length of the tunnel is 1473.31 m and the section size is 11.24 m × 8.7 m (width × height) (Fig. 1a). The bottom of the tunnel is located at elevations of 2253.00 m, and its geological section is shown in Fig. 1b. The main rock type of the tunnel is Biotite K-feldspar granite, which has a uniaxial compressive strength of 60–70 MPa, and pegmatite veins are relatively developed. The surrounding rock is mainly made of class IIIa and overall stability of the tunnel wall is satisfactory. The rock mass is mainly composed of a block structure. The local stability of the rock mass is poor. The deep buried section has a high in situ stress, and the maximum cover depth can reach 600 m. The SPD9 flat tunnel located at the elevations of 2267.6 m is an exploration tunnel excavated before tunnel excavation. According to the in situ stress measurement results of the SPD9 flat tunnel, the maximum principal stress σ_1 ranges from 15.98 MPa to 37.82 MPa, which indicates a high stress level. The detailed parameters of the in situ stress measurements are shown in Table 1. A drilling and blasting method was adopted to construct the access tunnel in the main powerhouse. When the stability of the surrounding rock is good, two blasting excavations are carried out in one day. When a blasting excavation is completed, the working surface is advanced by 2 m. We supported the rock mass with anchors. The diameter of the anchors is 25 mm and the length is 4.5 m. The longitudinal spacing and circumferential spacing of the anchors are both 2 m.

3. Establishment of microseismic monitoring system

To reveal the excavation-induced damage evolution law of the surrounding rock mass, a high sensitivity microseismic monitoring system, manufactured by the Engineering Seismology Group (ESG), Canada, was installed at access tunnel in the main powerhouse, as shown in Fig. 2. The microseismic monitoring system consists of a Paladin digital signal acquisition system, a Hyperion digital signal processing system, six uniaxial accelerometers, and signal transmission cables. The cables from all accelerometers were connected to a Paladin acquisition unit. The Paladin data acquisition system, using the STA/LTA algorithm with a threshold of 3, has an acquisition frequency of 20 kHz and a 24-bit analog-to-digital (A/D) converter. The accelerometers respond to frequencies in the range from 50 to 5 kHz, with a sensitivity of 30 V/g.

The accelerometers were cemented in the boreholes at the sidewalls using quick-hardening resin. The boreholes were 42 mm in diameter, and no less than 2 m in depth to decrease the disturbance of the background noise. According to the on-site construction conditions of the access tunnel in the main powerhouse and the optimum monitoring range of the accelerometers, six accelerometers were installed in three different sections and the interval of the accelerometers along the tunnel axis was 40 m, as shown in Fig. 2. When the working face was advanced for approximately 40 m, the last row of accelerometers was moved forward to the first row. The first row of accelerometers was designed to be no less than 50 m behind the working face to ensure the safety of personnel and microseismic monitoring equipment, and to be no more than 100 m to continuously capture the excavation unloading-induced microfracturing within the surrounding rock mass.

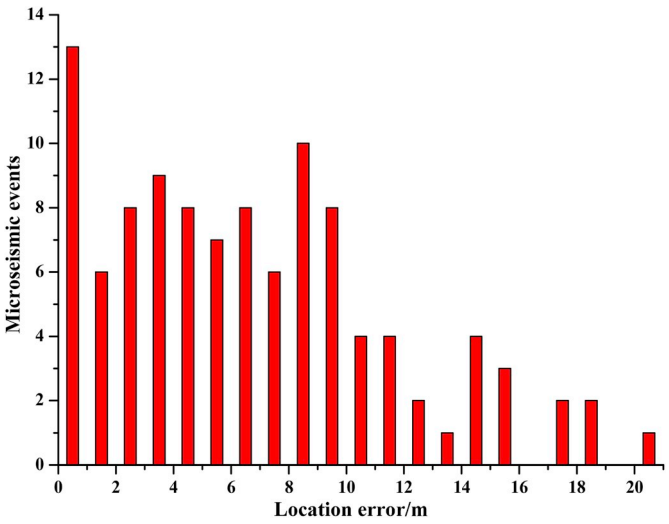

Fig. 4. Microseismic event location error distribution.

The microseismic monitoring system captured various kinds of signals, including microseismic events, blasting, rockbursts, and noise. Fast Fourier Transform (FFT) is a widely used spectral analysis method, because it can better reflect global spectral characteristics of signals. Fig. 3 shows some common signals in both time and frequency domains at the access tunnel in the main powerhouse. Note that the amplitude unit of the amplitude-time curve is set to V (Volt) and the amplitude unit of the amplitude-frequency curve represents the relative dimensionless scale of vibration. Effective microseismic events can be recognized by analyzing the waveforms in both time and frequency domains.

From January 2, 2018 to January 12, 2018, a total of 8 blasting excavations were completed. The working face advance was approximately 16 m, and a total of 106 effective microseismic events were detected in the project region. The number of microseismic events with a location error of less than 10 m accounted for 78.3% (Fig. 4), which indicated that the monitoring data could satisfy the precision requirement of stability evaluation of the surrounding rock of the tunnel on site.[20] Fig. 5 shows the temporal distribution of the microseismic events. The period from January 5 to January 9 was the microseismic event active period, which indicated that the stability of the surrounding rock mass was relatively poor. To some extent, the number of microseismic events can reflect the active state of the surrounding rock, but to have a more in-depth and comprehensive understanding of the rockburst mechanism and to determine a more accurate rockburst early warning period, it is necessary to analyze and summarize the multi-parameters of the source in detail.

4. Analysis of microseismic activity characteristics

4.1. Spatiotemporal distributions of the microseismic events

To clarify the spatial distribution characteristics of microcracks in the surrounding rock of the access tunnel in the main powerhouse, the spatiotemporal distribution characteristics of the monitored microseismic events must be analyzed. Fig. 6 shows the spatiotemporal distribution of microseismic events from January 3, 2018 to January 10, 2018, including before, during and after rockbursts. In Fig. 6, every colored circle represents a microseismic event; the size of the solid circle

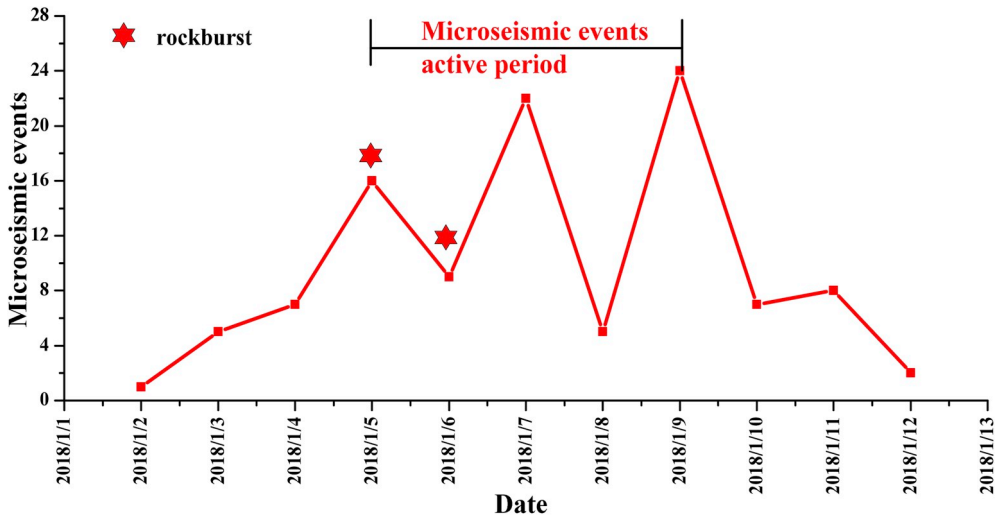

Fig. 5. Temporal frequency distribution of microseismic event.

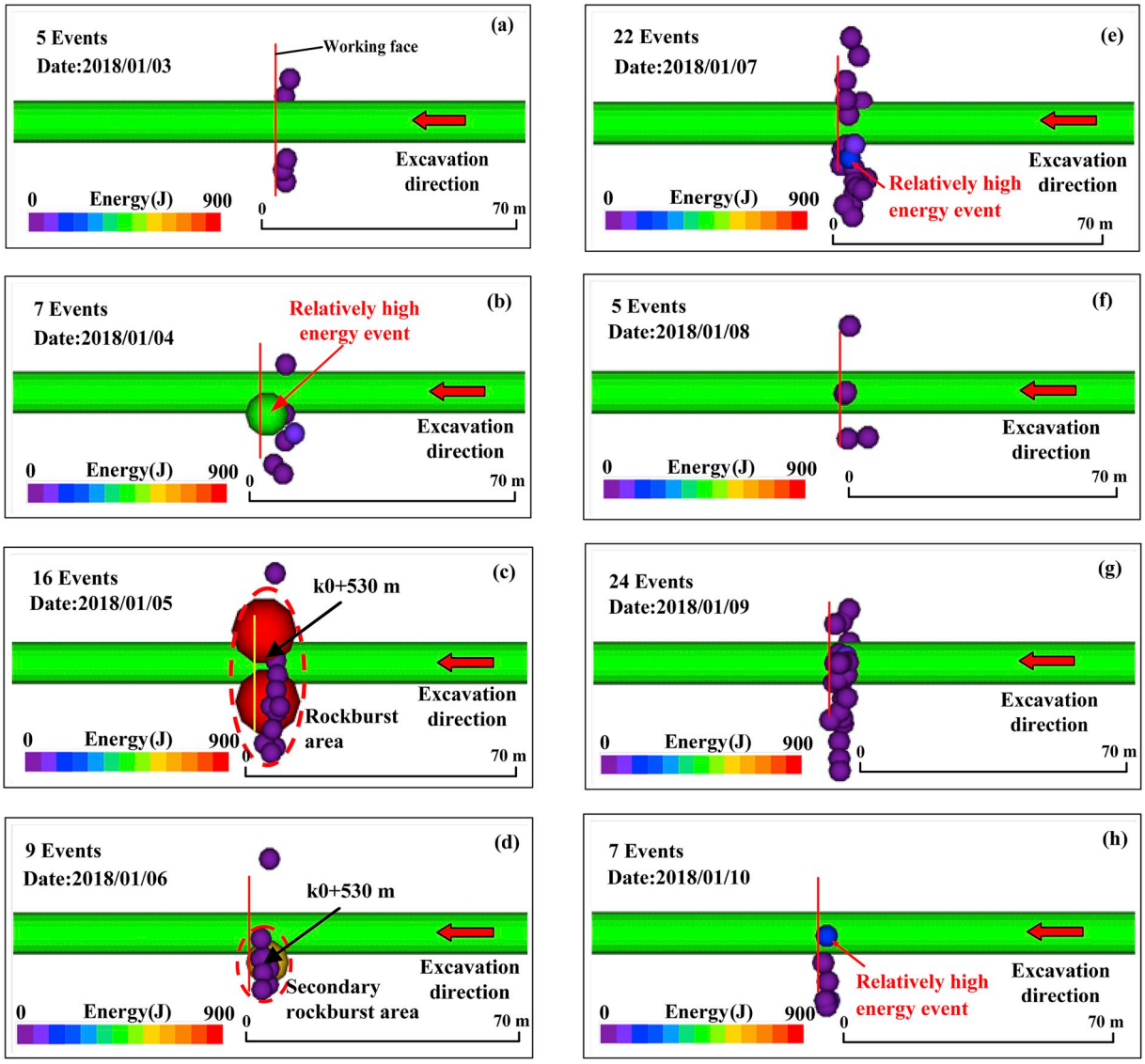

Fig. 6. Spatiotemporal distribution of microseismic events in rockburst region.

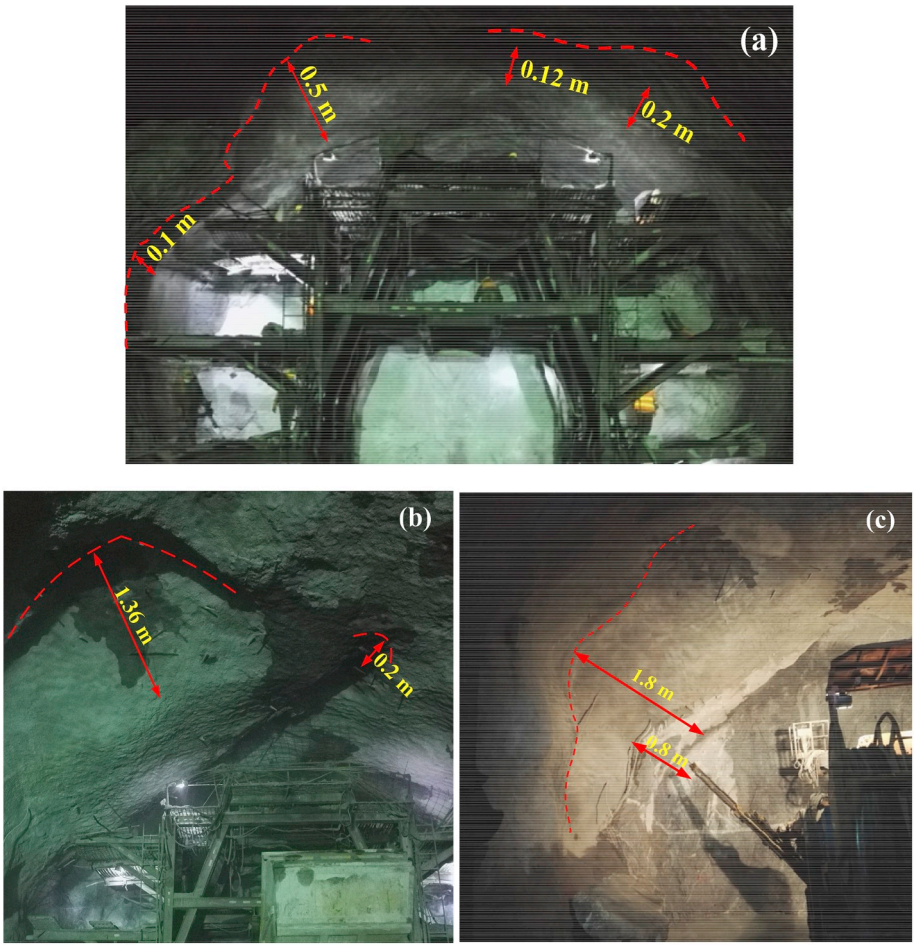

Fig. 7. Photos of surrounding rock mass damage after rockburst at Chainage k0+522 m-k0+532 m.

reflects the size of the energy released by the event; the specific value of the released energy is represented by the color.

On January 3, there were fewer microseismic events and the energy released was relatively low. The number of microseismic events increased on January 4, mainly concentrating in the left sidewall, and a relatively high-energy event occurred. Fig. 6b shows that the microcracks were mainly concentrated in the left wall of the tunnel, and the elastic energy stored in the surrounding rock was relatively high. The personnel on site could hear the sound of rock cracking from the left wall of the tunnel. At 7:04 on January 5, 2018, an excavation blasting event occurred at the working face. At 7:07 on January 5, 2018, a rockburst occurred at the right sidewall of the tunnel behind the working face, as shown in Fig. 6c. According to the analysis of the in situ stress direction and occurrence time, the rockburst was caused by the deformation resilience of the rock mass after unloading, and the released energy was relatively high. At 8:28 on January 5, 2018, an intense rockburst occurred at the left sidewall of the tunnel behind the working face, as shown in Fig. 6c. According to the analysis of the in situ stress direction and occurrence time, the rockburst was caused by the stress concentration of the rock mass after unloading. After blasting excavation, due to in-situ stress, the surrounding rock stress was redistributed, forming a local stress concentration region in the left sidewall of the tunnel. Local stress concentration resulted in the continuous initiation and expansion of microcracks, accompanied by energy transfer and accumulation.

When the surrounding rock accumulated enough energy, the rockburst occurred, releasing a large amount of energy. There was an intense "explosion" sound on site, and the depth of the rockburst failure was relatively deep, as shown in Fig. 7. After 35 h of blasting excavation, a rockburst occurred at 18:29 on January 6, as shown in Fig. 6d. The released rockburst energy was relatively low, occurring in the left sidewall of the tunnel, and the events on January 6 were mainly concentrated in the left sidewall of the tunnel. On January 7, a large number of microseismic events were induced by the excavation unloading again after the rockburst. The number of microseismic events continued to increase to 24 on January 9 after excavation unloading, but the energy released was relatively low. Fig. 6 shows that the microseismic events were mainly concentrated in the left side of the tunnel. Fig. 7 shows photos of surrounding rock mass damage after the rockburst at Chainage k0+522 m-k0+532 m. Due to the poor stability of this part of the rock mass, the steel bars were first used for random support, and then, the anchors were used for reinforcement support. The random supports were violently destroyed during the rockburst, as shown in Fig. 6. The maximum depth of rockburst failure was 1.8 m, which was caused by the continuous damage of the surrounding rock after the rockburst occurred. The severely damaged areas are mainly distributed in the left sidewall.

4.2. Cumulative apparent volume, the energy index and cumulative release energy

The energy index of an event is the ratio of the observed radiated seismic energy of that event to the average energy radiated by events of the same seismic moment with the event,[21] which is defined as follows:

$$EI = \frac{E}{\overline{E(M)}} \tag{1}$$

where E is the radiated seismic energy of an event, $\overline{E(M)}$ is the average

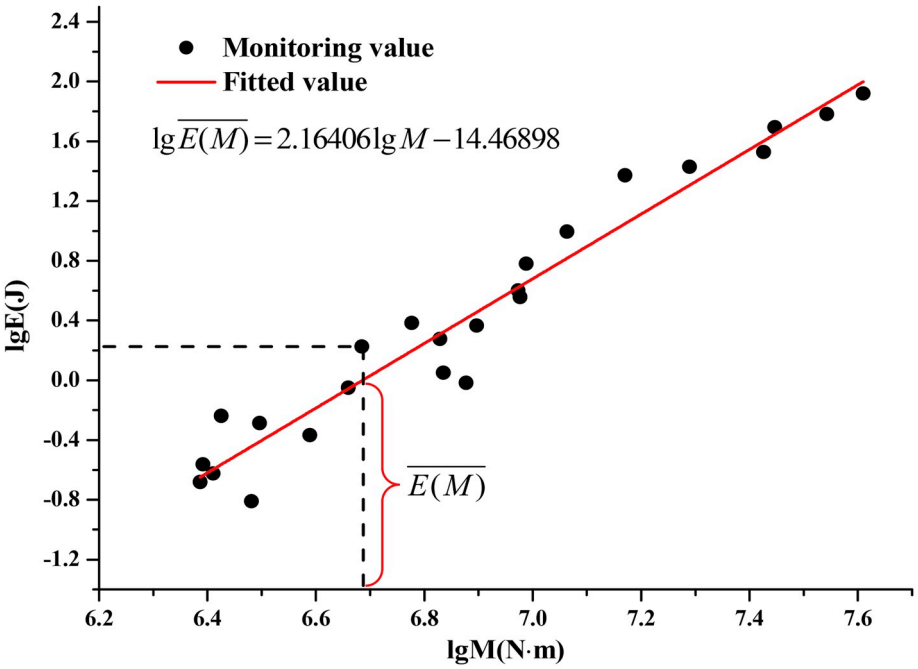

Fig. 8. Relationship between the energy and seismic moment of the microseismic events.

radiated seismic energy for a given seismic moment M, and EI is the energy index. The average radiated seismic energy can be taken from the relationship between $\lg\overline{E(M)}$and $\lg M$ for the area of interest

$$\lg\overline{E(M)} = c + d\lg M \tag{2}$$

where c and d are constants that can be calculated based on the relationship between the released seismic energy and seismic moment, as depicted in Fig. 8. The energy index can reflect the stress level in the monitoring region. An increase in the energy index means that the stress of the surrounding rock mass increases, implying an increased risk of rock instability.

The apparent volume, V_A, is the volume of a rock mass that experiences inelastic strain.[22] The apparent volume V_A can be obtained from

$$V_A = \frac{M}{2\sigma_A} \tag{3}$$

where M represents the seismic moment and σ_A is the apparent stress.

Based on the theory of rock mechanics instability, the characteristics of the temporal series curve of the energy index and apparent volume can be analyzed to reveal the activity law within the surrounding rock mass before, during and after a rockburst. The gradual increase of the energy index and the slow increase of the apparent volume indicate that the rock mass in the source region is stable, being in the strain-hardening stage of energy accumulation. After the peak strength of the rock, due to the decrease in rock bearing capacity, the stress decreases and the deformation increases. Correspondingly, the energy index decreases and the apparent volume increases, which indicates that the rock mass is strain-softening and is damaged.[23] Therefore, the analysis of the change characteristics of the energy index and the apparent volume is helpful in understanding rockburst mechanism and rockburst prediction.

Fig. 9a shows the entire rockburst process at the access tunnel in the main powerhouse of the Shuangjiangkou hydropower station. Because blasting excavation is very important for stress redistribution and stability analysis, the time positions of blasting excavations were marked in the figure. Fig. 9a shows four periods, namely, the stability period of the tunnel, the gestation period of the rockburst, the occurrence period of the rockburst and the occurrence period of the secondary rockburst. The cumulative apparent volume and cumulative released energy during the stability period increased slowly, without abrupt change, and the energy index curve had a small range of fluctuation. On January 4, when entering the rockburst gestation period, the energy index curve suddenly increased rapidly, while the cumulative apparent volume increased slowly, which indicated that the surrounding rock mass was in the strain-hardening stage of energy accumulation; then, the energy index sharply dropped and continued to decrease to a relatively low level, while the cumulative apparent volume continued to increase at a relatively fast speed, which indicated that the surrounding rock was in the strain-softening stage, and the local rock mass was damaged.[22] Subsequently, the energy index curve increased again sharply, and the cumulative apparent volume gradually increased, which indicated that local surrounding rock stress transferred to nearby surrounding rock, forming a new stress concentration region.

On January 5, two rockbursts occurred, all releasing relatively high energy. The first rockburst occurred 3 min after blasting excavation and the second rockburst occurred 1 h and 24 min after blasting excavation. According to the characteristics of temporal distribution, the blasting excavation directly induced the two rockbursts. The first rockburst occurred at 7:07:20; before the rockburst, the energy index began to increase gradually after a sharp decline, and the cumulative apparent volume gradually increased; the increment of the cumulative apparent volume was larger than that of the stable period and smaller than that of the gestation period. The energy released by the first rockburst event was 854.40 J, accounting for 45.47% of the total energy released on January 5. The second rockburst occurred at 8:28:48; before the rockburst occurred, the energy index curve also fluctuated greatly. The energy released by the second rockburst event was 853.22 J, accounting for 45.41% of the total energy released on January 5. The energy released by the two rockburst events on January 5 was relatively high, which was an abnormal situation, indicating that the energy accumulated in the surrounding rock mass was relatively high.

The analysis found that the energy index before the two rockbursts increased rapidly at first, then decreased rapidly, and then increased rapidly again; the cumulative apparent volume gradually increased. This result revealed that rockbursts generally included four processes: local rock mass compaction and stress concentration, rock mass damage and a transfer of part of the stress to the nearby rock mass, external disturbance, and rockburst. Blasting excavation can directly induce the

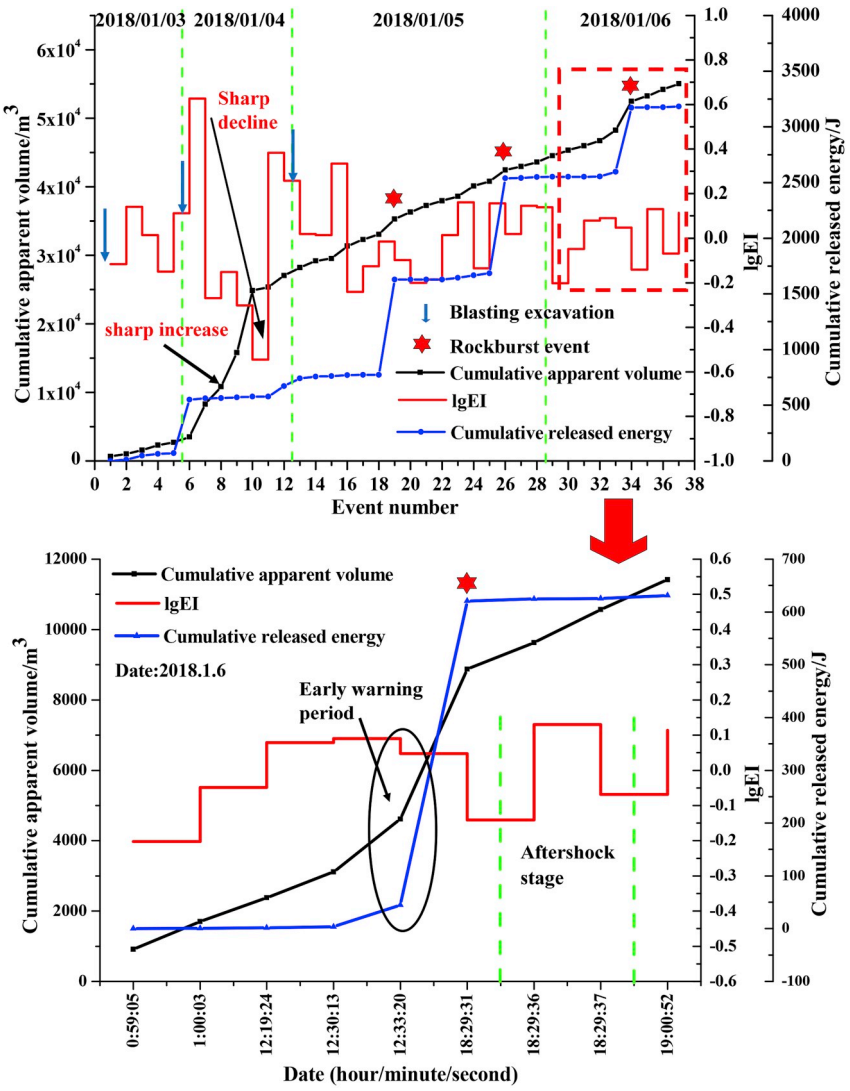

(a) Distribution characteristics of source parameters before and during rockburst.

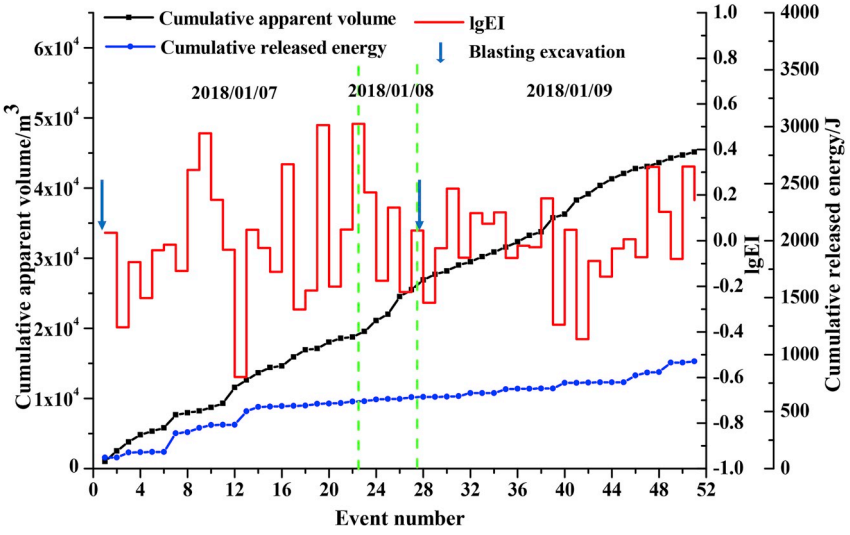

(b) Distribution characteristics of source parameters after rockburst.

Fig. 9. Cumulative apparent volume, energy index and cumulative released energy curves.

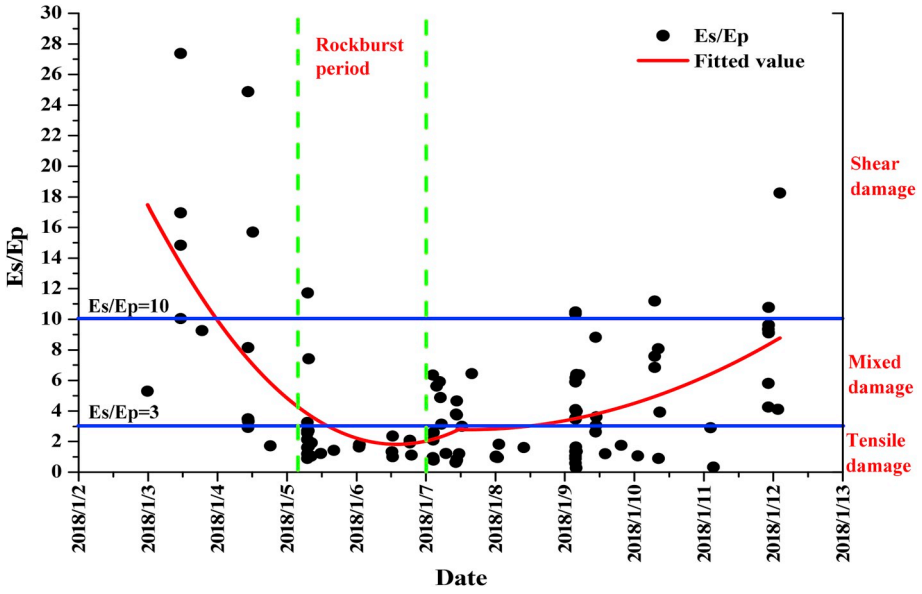

Fig. 10. Temporal distribution of Es/Ep values.

occurrence of rockbursts. In summary, the fluctuation of the energy index curve was relatively large, and the increment of the cumulative apparent volume was relatively large, which can be used as an early warning indicator of rockbursts.

There was no blasting excavation disturbance on January 6, 2018, and a rockburst occurred at 18:29. The rockburst was caused by the stress redistribution of the surrounding rock mass. From the comparison of energy index curves, it is found that the law of surrounding rock activity during the rockburst period on January 6 was significantly different from that during the rockburst period on January 5. In Fig. 9a, the contents inside the red rectangle were enlarged. On January 6, the energy index continued to increase, and the cumulative apparent volume also increased gradually, which was a typical strain-hardening energy storage stage. Then, the energy index suddenly dropped at 12:33:20 on January 6; however, the increment of cumulative apparent volume and cumulative released energy increased suddenly. This result indicated that the surrounding rock stress decreased, while the inelastic deformation volume increase of the surrounding rock was relatively fast, which is a typical early warning period of strain-softening.

Subsequently, effective microseismic events were not detected in the next 6 h. After the calm period, a rockburst occurred. The energy released by the rockburst event was 575.75 J, accounting for 91.22% of the total energy released on January 6. After the occurrence of the rockburst, the energy released by microseismic events was relatively low, while the energy index had a relatively large fluctuation; from the time distribution characteristics of events, this was determined to be an aftershock stage. Therefore, the increment of the cumulative apparent volume and the cumulative released energy of undisturbed rock mass suddenly increased, and the energy index suddenly decreased, which could be used as an early warning indicator of rockburst. The energy index of the rockburst event decreased, and the energy released by the rockburst event was relatively high, which indicated that a rockburst was indicated by the process of stress release and energy dissipation of the surrounding rock mass.

The study of the activity characteristics of the surrounding rock mass after rockburst is very important for guiding site construction, such as the regulation of construction schedules, and the safety of construction personnel and equipment. Fig. 9b shows the temporal series curve characteristics of the source parameters after the occurrence of rockburst. On January 7, a blasting excavation was completed, which was the first excavation disturbance of the surrounding rock mass after the occurrence of rockburst. It was found from the figure that the energy index curve had a relatively large fluctuation, the cumulative apparent volume increased gradually, and the cumulative released energy increased slowly. This result indicated that after the blasting excavation disturbance, the activity within the surrounding rock mass was relatively intense. The number of microseismic events was relatively large, and there was a slight rock rupture sound on site. The area of rockburst failure continued to increase.

Comprehensive analysis showed that the activity within the local surrounding rock mass was relatively active on January 7, so it was not suitable to continue blasting excavation construction. There was no blasting excavation disturbance on January 8, 2018. The fluctuation degree of the energy index curve on January 8 was smaller than that on January 7, while the increasing value of the cumulative apparent volume increased. This result indicated that the surrounding rock mass stability was still relatively poor. Because no high energy events occurred, the surrounding rock mass would not suffer from relatively severe instability. On January 9, a blasting excavation was completed, and the surrounding rock mass was again disturbed by excavation. On January 9, 24 effective microseismic events were captured, which was the most during the period from January 2, 2018 to January 12, 2018. The phenomenon of rock spalling was relatively serious, which verified the rationality of the prediction on January 8. From the comparison of the energy index curves, it was found that the stress activity of the surrounding rock mass was relatively stable, and the energy released by the events was relatively low on January 9 compared with that on January 7. The comprehensive analysis found that for the blasting excavation after the occurrence of rockburst, the number of microseismic events captured in a rock mass was relatively large, while the energy released by the events was relatively low. The rock block did not eject, and the area of rockburst failure continued to increase on site.

4.3. Ratio of S-wave energy to P-wave energy

In seismology, the ratio of the S-wave energy to the P-wave energy (E_S/E_P) is one of the important indexes reflecting the activity state of the surrounding rock mass. E_S/E_P can be used to judge the type of focal mechanism responsible for the generation of a microseismic event. Fletcher[24] found that events with a high E_S/E_P (greater than 10) are typically associated with fault-slipping or shearing, and events with an E_S/E_P less than 3 are associated with the tensile failure of rocks. Fig. 10 shows the temporal series distribution of E_S/E_P values before, during and after rockburst. Every solid circle represents a microseismic event. Curve

fitting of E_S/E_P values can reveal the dynamic response relationship between E_S/E_P values and rockburst.

In Fig. 10, the E_S/E_P values clustered in different regions in different time periods. The E_S/E_P values were relatively large before the rockburst occurred. On January 3, the surrounding rock mass was relatively stable, and the type of rock damage was mainly compression-shear damage. Leading up to the rockburst period, the E_S/E_P values gradually decreased, and the proportion of tensile damage of the surrounding rock mass gradually increased. When entering the rockburst period, that is, on January 5, two rockbursts were induced by blasting excavation; the E_S/E_P values mainly clustered in the region where the E_S/E_P values were less than 3; the type of surrounding rock mass damage was mainly tensile damage. When the rockburst occurred, the rock blocks ejected at a certain speed on site. On January 6, due to the adjustment of the surrounding rock mass stress, a rockburst occurred; the Es/Ep values were relatively small, and the type of surrounding rock mass damage was mainly tensile damage. After the occurrence of rockburst, on January 7, the Es/Ep values of some microseismic events were greater than 3; the Es/Ep values were still relatively small, so the stability of the surrounding rock mass was still relatively poor; a total of four relatively large-magnitude microseismic events were captured. After the occurrence of rockburst, the proportion of events with an E_S/E_P greater than 3 gradually increased over time, and on January 12, the E_S/E_P values clustered in the region where the E_S/E_P values were greater than 3. This result indicated that the surrounding rock mass tended to gradually stabilize. Therefore, the change characteristics of the E_S/E_P values can be used as an indicator for the rockburst warning of the surrounding rock mass of the tunnel.

The above results show the following rockburst mechanisms: Due to the excavation unloading effect in a high-stress environment, the surrounding rock mass will undergo a complex stress dynamic adjustment process, and finally, two active regions with different stress states will be formed. The surrounding rock mass activity characteristics of the stress concentration region were as follows: one direction was pressurized, while the other direction was unloading pressure by blasting excavation; due to the effect of the principal stress, the type of rock damage was mainly compression-shear damage in the stress concentration region, so the Es/Ep values of microseismic events were relatively large; at the same time, the rock mass in the direction of unloading stress began to expand, and the proportion of tensile damage of surrounding rock mass began to increase over time. In this process, as the tensile cracks continued to expand, penetrate and open, the rock mass near the wall of the tunnel initially formed a certain thickness of rock blocks or slices; the surrounding rock damage was transformed into tensile damage, so the E_S/E_P values were relatively small. When the rock blocks or slices had enough energy, they ejected at a certain speed, forming a rockburst, accompanied by the release of a large amount of energy.

After the rockburst occurred, the surrounding rock mass of the tunnel formed a new free face; due to the deterioration of the surrounding rock environment, the tensile cracks near the free face continued to expand, forming new rock blocks or slices to eject outward. As a result, the area of rockburst failure continued to expand into the surrounding rock mass, eventually forming a "V-shaped" rockburst failure region. Generally, the time interval between rockburst and blasting excavation was relatively long. The surrounding rock mass activity characteristics of the stress relaxation region were as follows: After the blasting excavation, the surrounding rock mass suddenly removed a relatively large stress; the rock mass had a deformation resilience, which was equivalent to a tensile stress on the free face; some new tensile cracks were formed in the surrounding rock mass; after the cracks continued to expand and penetrate, the rock mass was ejected at a certain speed. The rockburst failure region generally did not expand into the surrounding rock, so the depth of rockburst failure was relatively shallow. Generally, the time interval between the rockburst and blasting excavation was relatively short.

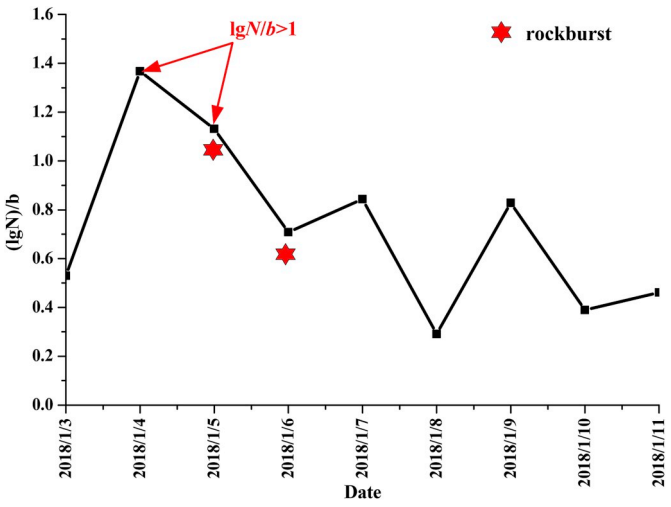

Fig. 11. Temporal distribution of lgN/b value.

4.4. Ratio of lgN to b

In 1944, Gutenberg and Richter[25] proposed a statistical relationship between earthquake magnitude and frequency in the seismic field. A large number of studies[26] based on field observations indicate that the moment magnitude and frequency of the microseismic events also obey the earthquake magnitude and frequency (Gutenberg-Richter) relationship, which is expressed as follows:

$$lgn = a - bm \tag{4}$$

where m is the magnitude, n is the number of earthquakes whose magnitude is no less than m, and a and b are constants. The b value represents the proportional relationship between the number of large magnitude events and the number of small magnitude events. When the b value increases, the proportion of the small-magnitude events increases, and the proportion of the large-magnitude events decreases, and vice versa. Therefore, the change in the b value can be used to reflect the change in the stress field of the surrounding rock mass. The b value of microseismic activity caused by stress adjustment usually ranges between 1.2 and 1.5.[27]

The larger the number of daily events N, the more microcracks will appear in the surrounding rock mass, the more intense the surrounding rock activity, and the greater the risk of surrounding rock mass instability. In this paper, based on the significance of the number of daily events N and the b value, lgN/b was first proposed as an indicator for predicting rockbursts. Fig. 11 shows the temporal distribution of lgN/b values of microseismic events.

In Fig. 11, on January 4, the rockburst early warning period, the lgN/b value increased sharply, reaching a maximum of 1.38. This result indicated that the surrounding rock mass stress was relatively high, and the number of microcracks was relatively large; at this time, the risk of rockburst of the surrounding rock mass was relatively high. On January 5, a blasting excavation was completed, which directly induced the occurrence of rockburst; there were two rockbursts in this day, accompanied by a large amount of energy release. On January 5, the value of lgN/b decreased, but it remained above 1; that is, the lgN/b value was still at a relatively high level. This result indicated that the risk of rockburst of the surrounding rock mass decreased, but the stability of the surrounding rock mass remained relatively poor. After a long period of surrounding rock mass activity, a rockburst occurred at 18:29:31 on January 6, releasing an energy of 575.75 J. Compared with the energy released by the rockburst events on January 5, the released energy of the rockburst event decreased on January 6. From January 6 to January 11, the lgN/b value was less than 1, so the rockburst risk decreased.

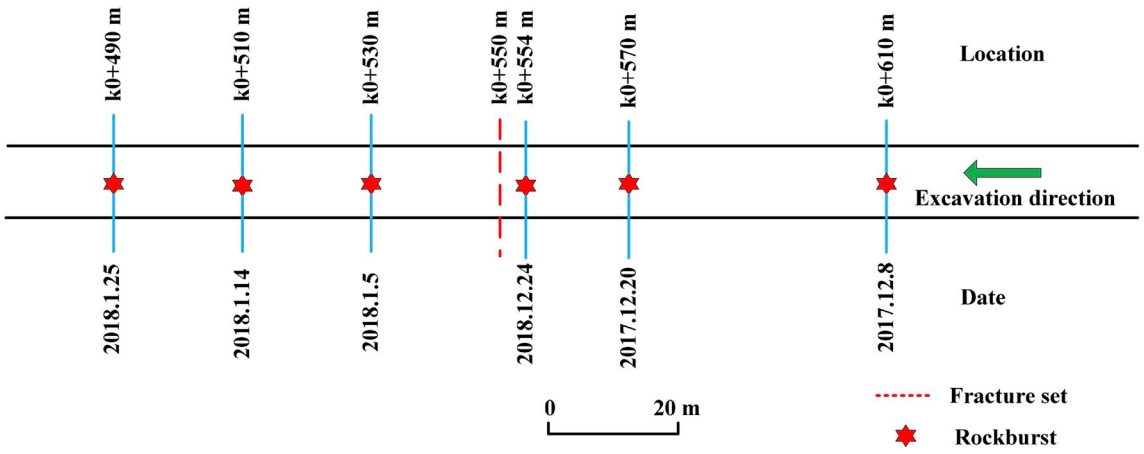

Fig. 12. Rockburst spatial distribution.

Table 2
LgN/b values before occurrence of rockbursts.

Date	2017.12.7	2017.12.19	2017.12.23	2018.1.4	2018.1.13	2018.1.24
lg*N/b*	1.2928	1.6728	1.0927	1.3678	1.0871	1.3266

However, the lg*N/b* value was still relatively high on January 6. When a blasting excavation was completed on January 7, the lg*N/b* value began to rise, which indicated that the surrounding rock mass stability deteriorated. No blasting excavation occurred on January 8, and the lg*N/b* value decreased significantly. On January 9, due to the blast excavation, the lg*N/b* value rose again. On January 10 and January 11, the lg*N/b* values were relatively low, which indicated that the surrounding rock stability was relatively good.

The above narrative indicates that the lg*N/b* value can be used as an indicator to evaluate the rockburst risk of the surrounding rock mass. When the lg*N/b* value was relatively high, the risk of rockburst was relatively high. When the lg*N/b* value was greater than 1, a rockburst generally occurred in a short period of time. On January 4, the lg*N/b* value was greater than 1, and a rockburst occurred on January 5; the lg*N/b* value was still greater than 1 on January 5, and a rockburst occurred on January 6 (Fig. 11). If there was a blasting excavation disturbance, the lg*N/b* value rose (Fig. 11) because blasting excavation led to energy accumulation of the surrounding rock mass. If a rockburst occurred, the lg*N/b* value decreased (Fig. 11) because the rockburst dissipated a lot of energy. From January 4 to January 6, it was found that the higher the lg*N/b* value, the more intense the rockburst, as depicted in Fig. 11. When the lg*N/b* value ranged between 0.8 and 1, rock blocks fell off on site but there were no ejections. The surrounding rock mass gradually tended to stabilize over time after the rockburst occurred (Fig. 11).

If the threshold value of lg*N*/b was set to 1, it can successfully predict the occurrence of some rockbursts in other tunnel sections, as shown in Fig. 12 and Table 2.

5. Conclusions

Through a detailed analysis and summary of the microseismic monitoring information in a rockburst tunnel section, a more accurate early warning period was determined, and the rockburst mechanism was revealed. Furthermore, a new source parameter lg*N/b* was introduced to predict the rockburst, and a new evaluation method for tunnel rockburst was established. The main conclusions are as follows:

The change characteristics of the energy index and the cumulative apparent volume temporal series curve can reflect the activity state of the surrounding rock mass. The sharp decrease in the energy index and the rapid increase in the cumulative apparent volume indicated the deterioration of the surrounding rock stability. On January 5, rockburst process could be divided into four stages, including local rock mass compaction and energy storage, rock mass damage and stress transfer, external disturbance, and rockburst. Therefore, the fluctuation of the energy index curve was relatively large, and the increment of the cumulative apparent volume was relatively large, which can be used as an early warning indicator of rockburst. On January 6, rockburst process could be divided into four stages, including rock mass damage and stress transfer, local rock mass compaction and energy storage, rock mass damage, and rockburst. Therefore, the increment of the cumulative apparent volume and the cumulative released energy the undisturbed rock mass suddenly increased, and the energy index suddenly decreased, which can be used as an early warning indicator of rockburst.

Based on the distribution characteristics of E_S/E_P values over time, the types of surrounding rock mass damage at various stages of rockburst were analyzed, revealing that the rockburst process underwent a transformation of compression-shear failure, tensile-shear mixing failure and tensile failure. When the type of surrounding rock damage was mainly tensile damage, the E_S/E_P values of the events were relatively low, and the risk of rockburst increased. This result indicated that the change in the damage type of the surrounding rock mass can also be used as an early warning indicator of rockburst.

The source parameter lg*N/b* was analyzed. The lg*N/b* value can be used as an indicator to evaluate the rockburst risk of the surrounding rock mass. The higher the lg*N/b*, the greater the rockburst risk. For the access tunnel in the main powerhouse of the Shuangjiangkou hydropower station, before the rockburst occurred, the lg*N/b* value was greater than 1; the higher the lg*N/b* value, the more severe the rockburst.

Detailed comparative analysis and summary of the multi-parameters of the source can more accurately and effectively judge the rockburst risk, and these research results provide a reference for regulating the excavation progress of the tunnel.

Declaration of competing interest

The authors declare that they have no known competing financial interests or personal relationships that could have appeared to influence the work reported in this paper.

Acknowledgements

This work was supported by the National Natural Science Foundation of China (No. 51779031, 51678170) and the Open Fund of State Key Laboratory of Coal Resources and Safe Mining of China (No. SKLCRSMI9KFA02), for which the authors are very grateful.

References

1 Zhang JJ, FU BJ. Rockburst and its criteria and control. *Chin J Rock Mech Eng*. 2008; 27(10):2034–2042.
2 Ortlepp WD, Stacey TR. Rock burst mechanisms in tunnels and shafts. *Tunn Undergr Space Technol*. 1994;9(1):59–65.
3 Kaiser PK, Mccreath DR, Tannant DD. *Canadian Rockburst Support Handbook*. Sudbury: Geomechanics Research Centre, Laurentian University; 1996.
4 Frid V. Calculation of electromagnetic radiation criterion for rock burst hazard forecast in coal mines. *Pure Appl Geophys*. 2001;158(5-6):931–944.
5 Romashov AN, Tsygankov S. Generalized model of rockbursts. Fiziko-Tekh nicheskie Problemy. *Probl Razrab Polezhy Iskop*. 1992;5, 29-5.
6 Liu ZB, Shao JF, Xu WY, Meng YD. Prediction of rock burst classification using the technique of cloud models with attribution weight. *Nat Hazards*. 2013;68(2): 549–568.
7 Gong FQ, Li XB. A distance discriminant analysis method for prediction of possibility and classification of rockburst and its application. *Chin J Rock Mech Eng*. 2007;26(5): 1012–1018.
8 Wang H, Ge M. Acoustic emission/microseismic source location analysis for a limestone mine exhibiting high horizontal stresses. *Int J Rock Mech Min Sci*. 2008;45 (5):720–728.
9 Xu NW, Li TB, Dai F, Zhang R, Tang CA, Tang LX. Microseismic monitoring of strainburst activities in deep tunnels at the Jinping II hydropower station, China. *Rock Mech Rock Eng*. 2016;49(3):981–1000.
10 Feng XT, Yu Y, Feng GL, Xiao YX, Chen BR, Jiang Q. Fractal behaviour of the microseismic energy associated with immediate rockbursts in deep, hard rock tunnels. *Tunn Undergr Space Technol*. 2016;51:98–107.
11 Feng GL, Feng XT, Chen BR, et al. A microseismic method for dynamic warning of rockburst development processes in tunnels. *Rock Mech Rock Eng*. 2015;48(5): 2061–2076.
12 Blake W, Leighton F, Duvall WI. Microseismic techniques for monitoring the behavior of rock structures. *Int J Rock Mech Min Sci*. 1975;12:69.
13 Xiao YX, Feng XT, Li SJ, Feng GL, Yu Y. Rock mass failure mechanisms during the evolution process of rockbursts in tunnels. *Int J Rock Mech Min Sci*. 2016;83:174–181.
14 Tang SH, Pan Y, Huang YH, et al. Application research of micro-seismic monitoring technology to geostress hazards in deep mining. *Chin J Rock Mech Eng*. 2009;28 (Supp.2):3597–3603.
15 Xiao YX, Feng XT, Chen BR, et al. Rockburst risk of tunnel boring machine part-pilot excavation in very strong rockburst section of deep hard tunnel. *Rock Soil Mech*. 2011;32(10):3111–3118.
16 Yu Y, Feng XT, Chen BR, et al. Fractal characteristics of micro-seismic volume for different types of immediate rock-bursts in deep tunnels. *Chin J Geotech Eng*. 2017;39 (12):2173–2179.
17 Chen BR, Feng XT, Zeng XH, et al. Real-time microseismic monitoring and its characteristic analysis during TBM tunneling in deep-buried tunnel. *Chin J Rock Mech Eng*. 2011;30(2):275–283.
18 Brown ET. Rockbursts: prediction and control. *Tunn Tunn*. 1984:3–17.
19 Ma TH, Tang CA, Tang SB, et al. Rockburst mechanism and prediction based on microseismic monitoring. *Int J Rock Mech Min Sci*. 2018;110:177–188.
20 Tang ZL, Liu XL, Li CY, et al. Microseismic characteristic analysis in deep TBM construction tunnels. *J Tsinghua Univ: Sci Tech*. 2018;58(5):461–468.
21 Van-aswegen G, Butler AG. Applications of quantitative seismology in South African gold mines//. In: *Proceedings of the 3rd International Symposium on Rockbursts and Seismicity in Mines*. Rotterdam: A A Balkema; 1993:261–266.
22 Mendecki AJ. Real time quantitative seismology in mines. In: *Proceedings of the International Symposium on Rockbursts and Seismicity in Mines. Kingston*. vols. 16–18. August 1993:287–295.
23 Tang LZ. *Study on Monitoring and Predietion of Seismicity and Rockburst in a Deep Mine*. Ph.D.Thesis. Changsha: Central South University; 2008.
24 Boatwright J, Fletcher JB. The partition of radiated energy between P and S waves. *Bull Seismol Soc Am*. 1984;74(2):361–376.
25 Gutenberg B, Richter CF. Frequency of earthquakes in California. *Bull Seismol Soc Am*. 1944;34(4):185–188.
26 Xu NW, Dai F, Zhou Z, et al. Study of characteristics of b-value for microseismic events in high rock slope. *Chin J Rock Mech Eng*. 2014;33(S1):3368–3374.
27 Legge NB, Spottiswoode SM. Fracturing and Microseismicity ahead of a deep gold mine stope in the pre-remnant stages of mining//. In: *Proceedings of the 6th International Congress on Rock Mechanics. Montreal:[s.n.]*. 1987:1071–1078.